Adaptation of the Hufnagel-Valley profile to non-sea-level ground altitudes

RAMON MATA CALVO,[1,*]

[1]*European Space Agency, Keplerlaan 1, 2201 AZ, The Netherlands*
**ramon.matacalvo@esa.int*

Abstract: Designing an optical ground network for satellite communications require an analysis of the turbulence impact in each potential location, to guarantee a desired availability. Knowledge of the turbulence conditions is crucial in designing mitigation techniques like adaptive optics or forward-error correction, and it has a direct impact on the margins assumed in the link budget calculations. The Hufnagel-Valley profile is widely used, to estimate the turbulence impact in a generic location due to its simplicity when measurements or detailed information is not available. A simple adaption of the Hufnagel-Valley profile is proposed to extend this model to the altitudes above the sea-level.

1. Introduction

In the last years, there has been an increasing interest on optical satellite communications. The large unregulated optical spectrum offers ground-to-space connectivity with high data-rate solutions for implementing feeder-links. These high-capacity links are currently using an almost saturated RF spectrum, mainly in Ka- or Ku-bands. Free-space optical communications is a promising alternative, due to its inherent secure, interference-free, and efficient transmission. Nevertheless, all these advantages are coupled with the challenge of cloud-free access and turbulent-resistant communications.

Cloud-free access can be guaranteed by a network of N ground-stations located in uncorrelated weather conditions [1]. Ideally, one single optical ground station can provide the required feeder-link capacity. The availability of the optical feeder-link is then driven by the probability of clear-sky conditions of a single optical ground station in that network. If multiple optical ground stations shall operate simultaneously, the number of locations must increase, to maintain the same target availability.

Turbulence-robust solutions require the use of adaptive optics and forward-error correction techniques tailored to the turbulent channel. Particularly time-diversity techniques like interleaving or erasure codes are needed to cope with the turbulence-induced fading. However, the satellite platform limitations on power and heat-dissipation impose relatively simple solutions on the signal processing, especially when targeting high amounts of data. Therefore, minimizing the turbulence impact is essential for achieving better performance, higher availability, and implementation viability.

The selection of the ground station is key in designing the ground station network. Optical ground stations must be located closer to terrestrial optical fiber access, rather than in remote areas. But. the location of each single optical ground station is crucial in terms of the turbulence conditions. Locations closer to the sea-level will suffer of stronger turbulence conditions than locations at e.g., astronomical sites, which usually are set at higher altitudes. An analysis of the operating turbulence conditions is mandatory to guarantee the desired system availability, but turbulence-profiles measurements are not available everywhere.

Multiple turbulence profiles have been published [11, 3]; a good overview of parametric and non-parametric turbulence profiles can be found in [4]. But the well-known Hufnagel-Valley profile remains the most agnostic choice, due to its analytical formula and the need of estimating only two parameters: the turbulence strength at sea level and the rms crosswind velocity. The first parameter affects the lower part of the turbulence profile, while the second the higher part. Due to its simplicity, it is the best option when no further information on the location is available.

However, the Hufnagel-Valley profile does not take into consideration the altitude of the optical ground station location. For optical ground stations located at altitudes above the sea-level, just cutting the profile at the desired height in the sky will lead to an underestimation of the turbulence impact. The boundary layer of the atmosphere contributes the most on the turbulence effects and it is known that its thickness remains quite constant with the altitude.

Measurements performed with satellite communication links at different altitude locations [5-7] did not show a strong dependency of the Fried parameter with respect to the ground-level altitude: i.e., 8-18 cm around 30 degrees elevation at ~580 m ground level altitude [5], a median of 14 cm between 30 and 60 degrees elevation at ~3000 m ground level altitude [6] and a median of 4-12 cm around 30 degrees elevation at 2470 m ground level altitude [7], The Fried parameter values are all referenced to 1550 nm. Despite the expected little impact on the turbulence parameters, including the altitude influence in the turbulence profile is interesting, especially in relative comparison between different possible locations, when analyzing the link budget for communications.

The objective of this paper is to propose a simple adaptation of the Hufnagel-Valley profile that scales the ground turbulence strength when the optical ground station is not located at sea-level. In that way, the impact of the ground-level altitude can be evaluated, without further assumptions on the turbulence strength at each location. The estimation of the Fried parameter and the isoplanatic angle are then compared to publicly available measurements taken in several locations around the world.

The following definitions are used in this document:

h: height with respect to sea-level

h_0: ground-level altitude: altitude of the ground-level with respect to sea-level. The optical ground station is located at this altitude.

$C_{n,0}^2$: refractive index structure parameter value sea-level.

C_{n,h_0}^2: refractive index structure parameter value at a ground-level heigh h_0.

H: represent the altitude of the highest atmospheric layer above the sea-level.

2. Scaling the ground-level turbulence parameter

The scaling of the structure parameter with the ground-level altitude is based on the barometric equation, which represents the change of pressure in altitude [11].

$$P = P_0 \left[\frac{T}{T_0}\right]^{\frac{gM}{RL_0}}$$

where g is the gravitational acceleration, M is the air's molar mass, R is the universal gas constant, L_0 is the temperature lapse rate, T_0 and P_0 are respectively the temperature and pressure at sea-level, and T and P are respectively the temperature and pressure at the desired altitude.

This formulation assumes a linear behavior of the temperature with the altitude. This is in line with the assumption that the temperature profile in the atmosphere is linear in chunks. Therefore, at the region where an OGS could be located (troposphere h<11km), the temperature change can be written as,

$$T = T_0 + L_0 h$$

The refractive index structure parameter C_n^2 is related to the temperature structure parameter C_T^2 by means of the pressure and temperature as follows [11]:

$$C_n^2 = \left(7.9 \cdot 10^{-5} \frac{P}{T^2}\right)^2 C_T^2$$

Combining it with the barometric equation, the change of the structure parameter for a ground location above sea-level is introduced as follows,

$$\frac{C_{n,h_0}^2}{C_{n,0}^2} = \left[\frac{T_0 + L_0 h_0}{T_0}\right]^{2\frac{gM}{RL_0}-4} \frac{C_{T,h_0}^2}{C_{T,0}^2}$$

where the linear change on the temperature with the altitude has been used again. C_{n,h_0}^2 and C_{T,h_0}^2 are respectively the refractive index and temperature structure parameters at h_0, and $C_{n,0}^2$ and $C_{T,0}^2$ are respectively the refractive index and temperature structure parameters at sea-level.

This equation depends on the change of the temperature structure parameter, but no modelling has been found in the literature, describing the change of this parameter with the altitude. Therefore, the only assumption that can be done is that at ground-level $\frac{C_{T,h_0}^2}{C_{T,0}^2} \cong 1$: i.e., the temperature structure parameter will remain constant when increasing the altitude of the ground level. The structure parameter C_T^2 has been measured in different locations and at different altitudes [8-10]. The change of the orography and type of soil or environment has larger impact on its value. Applying that assumption, the equation can be simplified to the following expression:

$$C_{n,h_0}^2 \cong C_{n,0}^2 \left[\frac{T_0+L_0 h_0}{T_0}\right]^{2\frac{gM}{RL_0}-4} \tag{1}$$

Considering standard values to the parameters, this equation can be written as

$$C_{n,h_0}^2 \cong C_{n,0}^2 [1 - \ 2.2523 \cdot 10^{-5} h_0]^{6.5298}$$

where $g = 9.8\, m/s^2$, $M = 0.02896\, kg/mol$, $R = 8.31446\, J/Kmol$, $L_0 = -0.00649\, K/m$ and $T_0 = 288.15\, K$

The Hufnagel-Valley structure parameter profile assumes the ground-level at the sea-level, also at zero meters. The crosswind velocity is represented by w and the turbulence structure parameter at sea-level by A.

$$C_n^2(h) = 0.00594 \left(\frac{w}{27}\right)^2 \left(\frac{h}{10^5}\right)^{10} exp\left(-\frac{h}{1000}\right) + \\ + 2.7 \times 10^{-16} exp\left(-\frac{h}{1500}\right) + A exp\left(-\frac{h}{100}\right)$$

An adaptation of the parameter A is required when introducing an altitude greater than zero for the ground -level. Furthermore, since the altitude vector will start at the altitude h_0, the exponent of the factor multiplying the parameter A is corrected, resulting in the following equation [11],

$$C_n^2(h) = 0.00594 \left(\frac{w}{27}\right)^2 \left(\frac{h}{10^5}\right)^{10} exp\left(-\frac{h}{1000}\right) + \\ + 2.7 \times 10^{-16} exp\left(-\frac{h}{1500}\right) + \\ + C_{n,0}^2 [1 - \ 2.2523 \cdot 10^{-5} h_0]^{6.5136} exp\left(-\frac{h - h_0}{100}\right) \qquad h \geq h_0 \tag{2}$$

The other terms in the equation, which describe the turbulence profile at higher altitudes, remain unchanged.

In the left plot of Figure 1 the ground-level C_n^2 with respect to the ground level altitude is shown. This plot. shows a slight decrease of the ground-level C_n^2, due to the temperature and pressure changes with the altitude. In the right plot of Figure 1, the modified Hufnagel-Valley profile is depicted for five altitudes: sea-level, 100-, 500-, 1000- and 2000-meters.

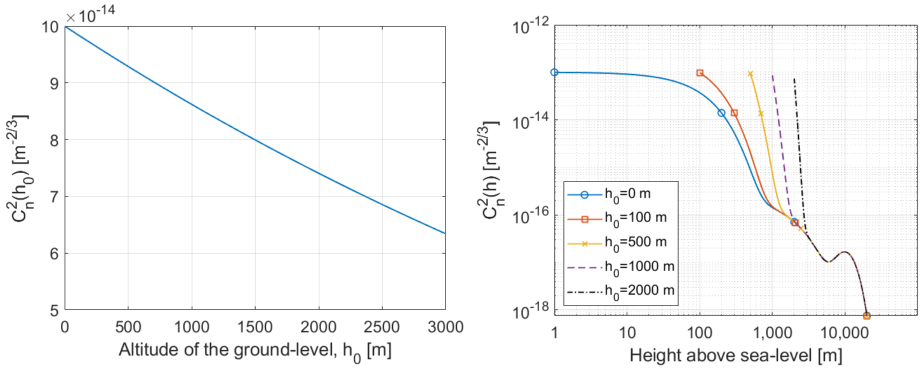

Figure 1. Left: change of the $C_n^2(h_0) = C_{n,h_0}^2$ (ground-level structure parameter) with the altitude. Right: modified Hufnagel-Valley profile for sea-level, 100-, 500-, 1000- and 2000-meters altitudes.

The thickness of the boundary layer can be defined as the height at which the turbulence strength decreases to the 1% of its initial value, as defined by [11]. Following this definition, the estimated thickness of the boundary layer by the Hufnagel-Valley profile at sea-level is around 232 meters. As mentioned in [11], referencing [12], the thickness of the boundary layer may change depending on the local sharpness of the mountain peaks and the base width of the summit. In that case, it may be useful to tune the decay of the turbulence profile, by introducing a "boundary layer thickness" parameter t_{BL}, defining the decay of the last term of equation (2) by a factor F_R.

$$C_{n,0}^2[1 - 2.2523 \cdot 10^{-5} h_0]^{6.5136} exp\left(-\frac{h-h_0}{x_{BL}t_{BL}}\right) \quad (3)$$

where x_{BL} is derived from this last term, assuming that its value is reduced a factor F_R, when $(h - h_0) = t_{BL}$.

$$x_{BL} = [ln(F_R[1 - 2.2523 \cdot 10^{-5} h_0]^{6.5136})]^{-1}$$

Note that this modification makes sense when one can assume that the last term of the profile is still the dominating one within the factor F_R of its original value.

3. Fried parameter and isoplanatic angle estimations

Using the modified Hufnagel-Valley profile in equation (2), the Fried parameter r_0 and the isoplanatic angle are calculated. The Fried parameter is calculated using the formula [13]:

$$r_0 = \left[0.423 \frac{k^2}{cos\zeta} \int_{h_0}^{H} C_n^2(h) dh\right]^{-3/5}$$

where ζ represents the zenith angle and k the wavenumber.

For the calculation of the isoplanatic angle θ_0 it has been used the following formula [13]:

$$\theta_0 = \left[2.914 \frac{k^2}{cos^{8/3}\zeta} \int_{h_0}^{H} C_n^2(h) \cdot (h - h_0)^{5/3} dh\right]^{-3/5}$$

Note that the integrals have been modified to consider the ground-level altitude. The integral must be performed along the propagation path, and not with respect to the sea-level altitude.

The left plot in Figure 2 shows the Fried parameter (circles) and the isoplanatic angle (squares) using two assumptions on the modified Hufnagel-Valley profile. The solid-lines are retrieved using the scaling of the ground-level turbulence as described before in equation (1), assuming $C_{n,0}^2 = 10^{-13} m^{-2/3}$. The dashed lines assume that the Hufnagel-Valley factor A remains constant, independently of the ground-level altitude h_0. Only the exponential factor is adapted to limit the integral above h_0. For those calculations the wavelength was set to 1550 nm, the link elevation angle to 30 degrees, and the crosswind velocity to 21 m/s.

The Fried parameter changes between 5 cm and 6.5 cm using the scaled C_{n,h_0}^2 value, whereas it remains almost constant when the C_{n,h_0}^2 is kept constant. This is expected as the main contribution to the Fried parameter is from the boundary layer, and we have verified that its thickness remains almost constant, when changing h_0. The isoplanatic angle increases due to the increase of the ground-level altitude, but in this case, the impact of the structure parameter scaling is negligible.

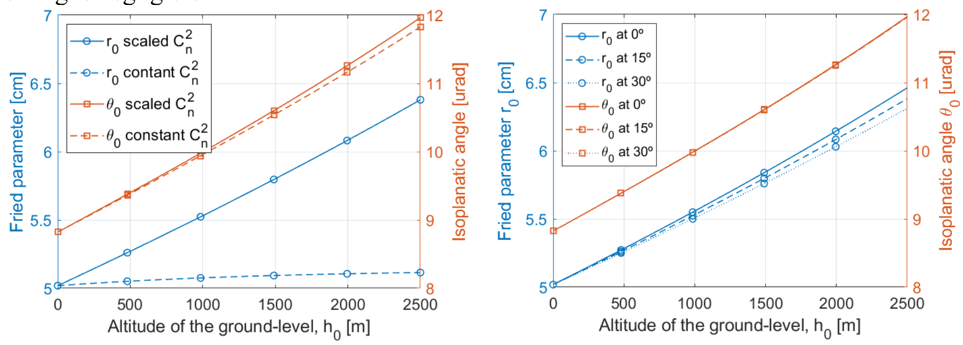

Figure 2. Fried parameter (squares) and isoplanatic angle (circles). Left: comparison of the scaled ground-level structure parameter with respect to the assumption of a constant value. Right: impact of the sea-level temperature change for 0, 15 and 30 degrees Celsius.

The right plot in Figure 2 shows the change of the Fried parameter (circles) and the isoplanatic angle (squares) with respect to the sea-level temperature. Taking the formulation of the structure parameter at ground-level in equation (1), the sea-level temperature was changed between 0 and 30 degrees. The plot shows that the sea-level temperature has little impact on the Fried parameter or the isoplanatic angle. Therefore, selecting 15 degrees as reference sea-level temperature is sufficient to estimate the turbulence profile.

The left plot in Figure 3 shows the change of the Fried parameter (circles) and the isoplanatic angle (squares) with respect to the ground-level altitude for two different boundary layer thicknesses. The solid lines represent a boundary layer of 232 m, as defined by the standard Hufnagel-Valley profile and the dashed lines makes use of equation (3) to set a boundary layer of 500 m. The boundary layer thickness is defined by the altitude at which the refractive index structure parameter is reduced by a factor of 100.

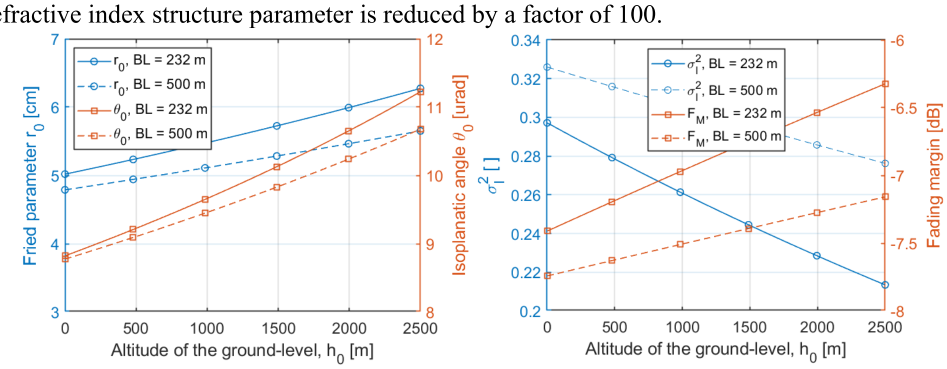

Figure 3. Left: Fried parameter (circles) and isoplanatic angle (squares). Right: uplink scintillation and fading margin (squares). Two different “boundary layer” thicknesses: 232 m (from standard Hufnagel-Valley profile) and 500 m has been considered.

In the right figure, the uplink scintillation (circles) and the fading margin (squares) are plot with respect to the ground-level altitude for the same two boundary layer thicknesses. For the scintillation a spherical wave was assumed and for the fading margin an out-of-service probability of 10^{-3}.

As expected, the increase of the ground-level altitude improves the atmospheric parameters, but the impact is relatively small. For example, for a ground-level altitude at 1000 m, compared to sea-level, there is an improvement of the fading level (considering only scintillation) by 0.5 dB, the Fried parameter by 0.5 cm and the isoplanatic angle by 1 µrad. However, when computing the link budget, considering all these effects together is still of interest.

4. Comparison with measured data

An empirical verification of this modification is not straightforward because it is not possible to isolate the influence of the ground-level altitude from other aspects tight-related to each location, like orography, soil type or vegetation, just to mention some examples. Therefore, the objective of this section is to determine if there is a general trend that validates the purpose of the proposed adaptation of the Hufnagel-Valley profile.

Based on published results of Fried parameter and isoplanatic angle measurements, a set of 13 locations were selected. Those locations are summarized in Table 1, including the acronym used in the figures, the altitude of each location, and the respective literature references. In the table it is indicated what measurements (Fried parameter or isoplanatic angle) are available and when they were performed (night or day). Most of the available data characterizes the Fried parameter (or seeing likewise) during the nighttime. Only few diurnal measurements of the Fried parameter were found. Isoplanatic angle measurements are also rare to find and unfortunately none of the references contained daytime measurements. Most of the statistically representative data is provided by astronomical observatories, which are located at high altitudes. Data at low altitudes is also rare to find and not always its statistical behavior can be properly derived.

Acronym	Location	Altitude [m]	Night	Day	r_0	θ_0	Ref
RO	Rongcheng	80.2	x		x	x	14
OP	Oberphaffenhofen	480	x		x		5
BA	Baikal Astrophysical Obs.	700		x	x		15
SSO	Siding Spring Observatory	1165	x		x		16
CO	Calern Observatory	1261	x		x	x	17
CA	Calar Alto Observatory	2168	x		x		18
TO	Teide Observatory	2390	x	x	x		19,20
TAOGS	Teide Observatory	2390		x	x		21
PA	Paranal	2635	x		x	x	22, 17
SPM	San Pedro Mártir	2800	x		x	x	23
DO	Delingha Observatory	3200	x	x	x		24
LH	Lhasa	3650	x		x	x	14
MK	Maunakea	4205	x		x	x	25, 17

Table 1. Selected locations for measurement comparisons.

In Figure 4, there is the comparison between the theoretical model in equation (2) for three turbulence conditions and with the measurements reported in the literature. The left plot depicts the Fried parameter and the right plot, the isoplanatic angle. The x-axis of both plots represents the altitude of the location, i.e., the ground-level altitude h_0. In the left plot, the theoretical lines are calculated by selecting the structure parameter values at sea-level $C_{n,0}^2 = C_n^2(h = 0)$: $10^{-13}m^{-2/3}$ (dashed line), $10^{-14}m^{-2/3}$ (solid line) and $10^{-12}m^{-2/3}$ (dotted line) with a rms crosswind velocity of 21 m/s in all three cases. The grey shaded areas correspond to the impact on changing the crosswind velocity between 12 m/s and 30 m/s. Note that the crosswind velocity has little impact on the dashed line, where the structure parameter is higher. In the right plot, the structure parameter value at sea-level is set to $10^{-14} m^{-2/3}$ and the three lines represent the crosswind velocities $w = 12\ m/s$ (dotted line), $21\ m/s$ (solid line) and $30\ m/s$ (dashed line). Note that the isoplanatic angle changes only very little with the ground-turbulence and therefore, only one structure parameter value was considered here.

As in the previous section, a link elevation of 30 degrees and a wavelength of 1550 nm were assumed. From a satellite communications point of view this is a common reference scenario. The wavelength matches with most common communications components from terrestrial networks and the elevation angle is taken usually as reference for the communications adaptive optics systems. All data collected from the literature was scaled accordingly to meet this reference scenario. As most of publicly available data in the references is expressed in terms of seeing ϑ, the Fried parameter was derived using the relationship: $r_0 = 0.98\,\lambda/\vartheta$.

In the plots the measurements from the 13 locations are represented as follows: the black lines with the dot (•) cover the range between the 1st and 3rd quartile, being the dot itself the median value. The blue circle (○) represents the mean value and when the line is drawn it covers the range defined by the mean value ± the standard deviation. The red lines with the cross (×) represent a range of values, not related to statistical parameters. This last category is included because the related references provide daytime information, which is not usual to find in literature. The location names are identified by its acronym, as listed in Table 1, adding "n" as subindex when it represents nighttime measurements and "d" for daytime. For data containing both night and daytime experiments no subindex was added.

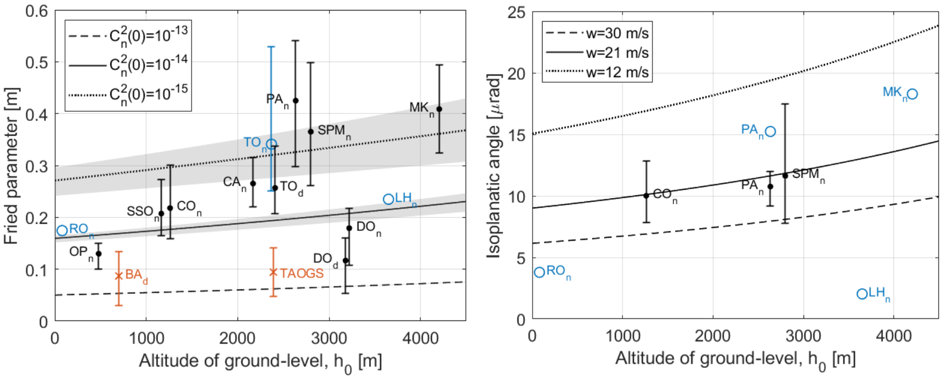

Figure 4. Left: Fried parameter. Right: isoplanatic angle. Comparison between the theoretical model of equation (2) and measurements from 13 locations. The values are calculated for a link elevation of 30 degrees and a wavelength of 1550 nm.

In general, Figure 4 show the expected trend of larger Fried parameter and isoplanatic angle when the altitude of the location h_0 increases. Furthermore, there is a good agreement with the theoretical curves calculated from the proposed modified turbulence profile, with Paranal (PA), San Pedro Mártir (SPM) and Maunakea as the largest outliers for the Fried parameter.

At the first three locations (Rongchen, Oberpfaffenhofen and Baikal) available data is little statistical representative due to their limited number of samples or missing analysis. However, they provide a picture of the turbulence impact at low altitudes, difficult to find in publications.

Using sounding balloons, measurements were performed in Rongchen (RO) in China for one week [14] in the evening or early in the morning. These median values will be compared with other ones taken in Lhasa, at much higher altitude, using the same method. Note that most of days were cloudy when measurements were taken. This reference also includes an estimation of the isoplanatic angle, which does not agree with the model.

The measurements in Oberpfaffenhofen (OP) [5] were taken between 0 AM and 1:30 AM UTC, the hours when larger turbulence is expected at night. The data was extracted from the mentioned paper, scaled accordingly with the link elevation and an empirical cumulative distribution function (CDF) was computed.

At the Baikal Astrophysical Observatory (BA) a set of measurements were performed in daytime [15]. In the paper the mean, the median and the standard deviation were computed for each season: winter, spring, summer, and fall, covering a total of 48 days. The combined statistics over the whole year and the quartiles were not found. Therefore, it was decided to represent a range of values: the cross is the mean value of all seasons, and the line covers the range defined by the minimum mean seeing value (winter) minus its standard deviation and the maximum mean seeing value (summer) plus its standard deviation. It is interesting to notice that the values are located clearly in the lower part of the plot, where the stronger turbulence conditions are expected.

The references for Siding Spring Observatory (SSO) in Australia [16], Calern Observatory (CO) in France [17] and Calar Alto Observatory (CA) in Spain [18] provide CDFs, from which the quartiles can be derived. All measurements are taken in nighttime. For SSO the CDF with larger number of data was selected, representing 7 days in June 2006. The CO reference [17] provided the CDF of more than 5 years data and CA reference almost 3 years. Furthermore, isoplanatic measurements were performed at CO in the same period, which makes this location very interesting when comparing both parameters at the same time.

At the Teide Observatory (TO) there are three references reporting measurements: at night (TO_n) [19], in the day (TO_d) [20] and combining both night and day (TAOGS) [21]. For the measurements at night, TO_n, only the mean value and standard deviation were reported, covering roughly 3 moths in the winter with 2228 samples. The TO_d measurements were performed only in daytime, covering 24 days in July 2021 and their CDF was provided. Both measurements TO_n and TO_d were collected using turbulence monitoring systems and they seem to be coherent each other, i.e., in the daytime the Fried parameter is lower. Finally, Fried parameters measurements during day and night were performed using the adaptive optics system of the Transportable Adaptive Optics System (TAOGS), located in the Teide Observatory, and covering all four seasons. The reference [21] reports the median evolution during night and daytime but no other statistics are provided. In Figure 4 the marker reports the span of these median values. There is a clear difference between the first set of measurements $TO_{n,d}$ and the ones provided in TAOGs. It is worthwhile to note that the method and the hardware configuration used by the TAOGS and by $TO_{n,d}$ are different.

Measurements performed in Paranal (PA) [22] and in San Pedro Mártir (SPM) [23] are reported using CDFs. In PA the measurements cover almost 1,5 years, whereas in SPM only few weeks. The Fried parameters provided by these datasets are not well represented by the proposed model, tending to overestimate the turbulence impact in both cases. For the isoplanatic angle the measurements at both locations seems to align their trend with the measurements at CO using the theoretical curves. In Figure 4 the Paranal isoplanatic angle from GSM database [17] is included in the right plot with a blue circle.

Measurements have been performed on the Tibetan plateau, in the Delingha Observatory (DO) at night DO_n and daytime DO_d, as reported in [24] and in Lhasa (LH) [14]. The DO measurements cover 208 days in three years, mainly between spring and autumn and the CDFs are provided. The LH measurements cover one week, and they were performed using a sounding balloon like the Rongchen measurements and only the median value is provided. Like in RO, most of days were cloudy as the measurements were performed. The Fried parameter measurements at DO in night and daytime agree each other, but compared to Paranal or San Pedro Mártir, they represent clearly much worse turbulence conditions. The LH Fried parameter agrees with the RO measurement and with the DO_n values. The LH reference is also providing an estimation of the isoplanatic angle, but the measurement does not follow the expected trend in the altitude; better isoplanatic angle would be expected at higher altitudes because of the reduced path through the atmosphere, as the other three references show.

Furthermore, both RO and LH isoplanatic angles are well below to the values predicted by the theory and reported in other locations.

Finally, seeing measurements from Mauna Kea (MK) were directly downloaded from the Mauna Kea Weather Center (http://mkwc.ifa.hawaii.edu), but they are also published in [25]. The CDF over 3518 nights have been considered. In this case, the model also does not fully cover this location. In Figure 4 the isoplanatic angle from GSM database [17] is included in the right plot with a blue circle. This value and PA_n from the same reference agree with the improvement estimated by the theoretical model.

Generally, the trend defined by the proposed model follows the trend of the published measurements. Finding a match between theory and measurements at all locations was not the purpose, but rather showing that the proposed modification provides a reasonable trend for the calculated parameters when changing the ground-level altitude. Figure 4 shows that astronomical locations on top of a mountain like TO, SPM, PA and MK have advantage with respect to other ones, where the elevation with the surrounding areas is less high, like OP, LH or DO, as one may expect. That may also explain the difference in the trends between these groups of locations.

5. Conclusions

In summary, a simple modification to the Hufnagel-Valley profile has been proposed to take the altitude into account. This modification is useful when analyzing the turbulence impact for optical satellite communications in locations where measurements or little information is available. The proposed modifications include the scaling of the ground turbulence structure parameter with the altitude and enabling the change of the turbulence decay in the lower part of the profile by defining an atmospheric boundary layer thickness.

The impact of the ground-level altitude on the Fried parameter and the isoplanatic angle have been compared to published measurements in 13 different locations, showing that the trend in the improvement of these parameters is predicted by the theoretical model. Orography and local characteristics of each location will influence specially when calculating atmospheric parameters, but the model provides a conservative estimation that is very valuable when no other information on the location is available.

Acknowledgments. The author wants to thank David Alaluf and Constanze Seibert for the valuable discussions and their suggestions.

Disclosure. This work has been started at the German Aerospace Center (DLR) and concluded in the European Space Agency (ESA). The author declares no conflicts of interest.

Data availability. Data underlying the results presented in this paper are not publicly available at this time but may be obtained from the authors upon reasonable request.

References

1. C. Fuchs, S. Poulenard, N. Perlot, J. Riedi, J. Perdigues, Optimization and throughput estimation of optical ground networks for LEO-downlinks, GEO-feeder links and GEO-relays, Proc. SPIE 10096, Free-Space Laser Communication and Atmospheric Propagation XXIX, 1009612, 2017
2. F. G. Smith, Atmospheric propagation of radiation, The infrared & electro-optical systems handbook Volume 2, SPIE Press, 1993
3. L. C. Andrews, R. L. Phillips, D. Wayne, P. Sauer, T. Leclerc, R. Crabbs, Creating a Cn2 profile as a function of altitude using scintillation measurements along a slant path, Proc. SPIE 8238, 2012
4. L. Canuet, Atmospheric turbulence profile modeling for satellite-ground laser communication, Master Thesis, Universitat Politècnica de Catalunya, 2014
5. N. Perlot, M. Knapek, D. Giggenbach, J. Horwath, M. Brechtelsbauer, Y. Takayama, T. Jono, Results of the optical downlink experiment KIODO from OICETS satellite to optical ground station Oberpfaffenhofen (OGS-

OP)", Proc. SPIE 6457, Free-Space Laser Communication Technologies XIX and Atmospheric Propagation of Electromagnetic Waves, 645704, 2007
6. M. Gregory, D. Troendle, G. Muehlnikel, F. Heine, R. Meyer, M. Lutzer, R. Czichy, Three years coherent space to ground links: performance results and outlook for the optical ground station equipped with adaptive optics, Proc. SPIE 8610, Free-Space Laser Communication and Atmospheric Propagation XXV, 861004, 2013
7. K. Saucke, C. Seiter, F. Heine, M. Gregory, D. Tröndle, E. Fischer, T. Berkefeld, M. Feriencik, M. Feriencik, I. Richter, R. Meyer, The Tesat transportable adaptive optical ground station, Proc. SPIE 9739, Free-Space Laser Communication and Atmospheric Propagation XXVIII, 973906, 2016.
8. C. R. Wood, R. D. Kouznetsov, R. Gierens, A. Nordbo, L. Järvi, M. A. Kallistratova, J. Kukkonen, On the Temperature Structure Parameter and Sensible Heat Flux over Helsinki from Sonic Anemometry and Scintillometry. J. Atmos. Oceanic Technol., 30, 1604–1615,2013
9. K. E. Kunkel, D. L. Walters, G. A. Ely, Behavior of the Temperature Structure Parameter in a Desert Basin. J. Appl. Meteor. Climatol., 20, 130–136, 1981.
10. D. A. Erasmus, L, A. Thompson, Ground turbulence at Mauna Kea Observatory: location and ground height for future telescopes, Proc. SPIE 0628, Advanced Technology Optical Telescopes III, 1986
11. R. B. Stull, An Introduction to boundary layer meteorology, Springer Dordrecht, 1988
12. R. Lynds, J. W. Goad, Observatory-site reconnaissance, Publications of the Astronomical Society of the Pacific, 96, 750-766, 1984
13. L. C. Andrews, R. L. Phillips, Laser beam propagation through random media, SPIE Press, 2005
14. Su Wu, Qike Yang, Jiangyue Xu, Tao Luo, Chun Qing, Changdong Su, Chan Huang, Xiaoqing Wu and Xuebin Li, A reliable model for estimating the turbulence intensity and integrated astroclimatic parameters from sounding data, MNRAS 503, 5692–5703, 2021
15. L. A. Bolbasova, A. Yu. Shikhovtsev, E. A. Kopylov, A. A. Selin, V. P. Lukin and P. G. Kovadlo, Daytime optical turbulence and wind speed distributions at the Baikal Astrophysical Observatory, MNRAS 482, 2619–2626, 2019
16. Michael Goodwin, Charles Jenkins and Andrew Lambert, Characterisation of the Optical Turbulence at Siding Spring, Publications of the Astronomical Society of Australia (PASA), Vol. 30, e009, 18 pages, 2013
17. Eric Aristidi, Yan Fantéï-Caujolle, Aziz Ziad, Julien Chabé, Christophe, Giordano, Catherine Renaud and Alohotsy Rafalimanana, Turbulence monitoring at Calern observatory with the generalized differential image motion monitor, Proc. SPIE 11448, Adaptive Optics Systems VII, 114487K, 2020
18. A. Ziad, R. Gredel, J. Aceituno, J. Borgnino, F. Hoyo, A. Irbah, F. Martin, U. Thiele and S. Pedraz, A site-testing campaign at the Calar Alto Observatory with GSM and DIMM instruments, Mon. Not. R. Astron. Soc. 362, 455–459, 2005
19. A. Varela, C. Muñoz-Tuñón, and A. de Gurtubai, Site-testing results at the Teide Observatory, ASP Conference Series, Vol. 266, 2002
20. Florian Quatresooz, Danielle Vanhoenacker-Janvier, and Claude Oestges, Daytime forecast of optical turbulence for optical communications, Communications and Observations through Atmospheric Turbulence (COAT) 2023, Durham, 2023
21. K. Saucke, J. Woicke, R. Mahn, T. Marynowski, P. Martin Pimentel, F. Heine, J. Surof, A. Reeves, R. Mata-Calvo, "Characterisation of the optical channel GEO to ground: using five years of data from Alphasat TDP1 and T-AOGS for investigation of different conditions," Proc. SPIE 11852, International Conference on Space Optics — ICSO 2020, 118525W, 2021
22. J. Osborn and M. Sarazin, Atmospheric turbulence forecasting with a general circulation model for Cerro Paranal, MNRAS 480, 1278–1299, 2018
23. R. Avila, E. Masciadri, J. Vernin, and L. J. Sánchez, Generalized SCIDAR Measurements at San Pedro Mártir. I. Turbulence Profile Statistics, Publications of the Astronomical Society of the Pacific, 116:682–692, 2004
24. Liming Zhu, Hanjiu Zhang, Liang Zhang, Xuefeng Duan, Xinying Lu, Ying Liu, Xuebin Li, Gang Sun and Ningquan Weng, Astronomical seeing and ground-level optical turbulence at Delingha observatory on the northern Tibetan Plateau, MNRAS 525, 3236–3247, 2023
25. Ryan Lyman, Tiziana Cherubini and Steven Businger, Forecasting seeing for the Maunakea Observatories, MNRAS 496, 4734–4748, 2020